Journal of Experimental Botany
https://doi.org/10.1093/jxb/erab525 Advance Access Publication 29 November, 2021

RESEARCH PAPER

Interactions between a mechanosensitive channel and cell wall integrity signaling influence pollen germination in *Arabidopsis thaliana*

Yanbing Wang[1,2,*], Joshua Coomey[1,2], Kari Miller[1], Gregory S. Jensen[1,†] and Elizabeth S. Haswell[1,2,‡]

[1] Department of Biology, Washington University in St. Louis, St. Louis, MO 63130, USA
[2] NSF Center for Engineering Mechanobiology
* Present address: Center for Applied Genetic Technologies, University of Georgia, Athens, GA 30602, USA
† Present address: Donald Danforth Plant Science Center, St. Louis, MO 63132, USA

‡ Correspondence: ehaswell@wustl.edu

Received 8 September 2021; Editorial decision 23 November 2021; Accepted 27 November 2021

Editor: Anna Dobritsa, Ohio State University, USA

Abstract

Cells employ multiple systems to maintain cellular integrity, including mechanosensitive ion channels and the cell wall integrity (CWI) pathway. Here, we use pollen as a model system to ask how these different mechanisms are interconnected at the cellular level. MscS-Like 8 (MSL8) is a mechanosensitive channel required to protect *Arabidopsis thaliana* pollen from osmotic challenges during *in vitro* rehydration, germination, and tube growth. New CRISPR/Cas9 and artificial miRNA-generated *msl8* alleles produced unexpected pollen phenotypes, including the ability to germinate a tube after bursting, dramatic defects in cell wall structure, and disorganized callose deposition at the germination site. We document complex genetic interactions between *MSL8* and two previously established components of the CWI pathway, *MARIS* and *ANXUR1/2*. Overexpression of *MARIS*^{R240C}*-FP* suppressed the bursting, germination, and callose deposition phenotypes of *msl8* mutant pollen. Null *msl8* alleles suppressed the internalized callose structures observed in *MARIS*^{R240C}*-FP* lines. Similarly, *MSL8-YFP* overexpression suppressed bursting in the *anxur1/2* mutant background, while *anxur1/2* alleles reduced the strong rings of callose around ungerminated pollen grains in *MSL8-YFP* overexpressors. These data show that mechanosensitive ion channels modulate callose deposition in pollen and provide evidence that cell wall and membrane surveillance systems coordinate in a complex manner to maintain cell integrity.

Keywords: *Arabidopsis thaliana*, callose, cell wall integrity, mechanosensitive ion channel, pollen.

Introduction

Cell mechanobiology includes the study of mechanical properties of cell constituents and the forces applied to or generated by cells and their microenvironment (Bidhendi and Geitmann, 2019). Plant cells perceive and respond to multiple external or internal forces important for their growth, survival, and development (Monshausen and Haswell, 2013; Trinh *et al.*, 2021).

Pollen, the male gamete of flowering plants, is an excellent model system for the study of plant cell mechanobiology due to its relatively simple structure, its unique biology, and the availability of *in vitro* growth systems (Johnson *et al.*, 2019). This single cell harbors two sperm cells and germinates a tube to deliver the sperm to the female ovule for double fertilization, navigating multiple osmotic and mechanical challenges during rehydration, germination, tube growth, and fertilization (Firon *et al.*, 2012; Adhikari *et al.*, 2020).

The plasma membrane is an important platform for mechanoresponses and it is expected that changes in the physical properties of the membrane result from changes in turgor or in cell wall integrity (CWI; Ackermann and Stanislas, 2020). A conserved mechanism for force perception at the membrane is the activation of mechanosensitive channels through increased membrane tension (Naismith and Booth, 2012; Peyronnet *et al.*, 2014; Ranade *et al.*, 2015). In plants, members of the MscS-like (MSL) family of mechanosensitive ion channels are localized to mitochondrial, plastid, and plasma membranes (Basu and Haswell, 2017), where they function as tension-regulated osmotic safety valves (Wilson *et al.*, 2011; Hamilton *et al.*, 2015; Hamilton and Haswell, 2017), some with additional complex functions (Veley *et al.*, 2014; Maksaev *et al.*, 2018). MSL8 is localized to the plasma membrane of pollen grains and tubes, and mediates mechanosensitive channel activities with a slight preference for anions (Hamilton *et al.*, 2015). MSL8's tension-sensitive ion transport activity is required to protect Arabidopsis pollen from osmotic challenges during *in vitro* pollen rehydration, germination, and tube growth (Hamilton and Haswell, 2017). Loss of MSL8 causes pollen grain to burst (Hamilton *et al.*, 2015).

The plant cell wall provides tensile strength and protection against both internal and external mechanical stresses (Höfte and Voxeur, 2017). The cell wall in a mature pollen surface comprises an inner intine wall, an outer exine wall, and a pollen coat. Callose, a polysaccharide in the form of β-1,3-glucan with some β-1,6-branches (Chen and Kim, 2009), is abundant in immature pollen grains, but disappears during pollen maturation and desiccation (Xu *et al.*, 2016). Pectic polysaccharides are critical and dynamic components of the pollen cell wall during all stages of development (Ma *et al.*, 2021). Once a pollen grain has rehydrated and is about to germinate, tube emergence begins with the formation of a germination plaque (Johnson and McCormick, 2001; Hoedemaekers *et al.*, 2015). This lens-shaped plaque is typically restricted to one site on the grain periphery. It contains callose, which is thought to add flexibility to the cell wall and increase its load-bearing ability, as well as cellulose and pectin (Johnson and McCormick, 2001; Parre and Geitmann, 2005; Hoedemaekers *et al.*, 2015). Pectin has been proposed to function as a hydrogel to control the influx of water into the grain during hydration (Vieira and Feijó, 2016). During germination, the germination plaque protrudes and extends, eventually forming the tip-growing tube that will ultimately deliver the male gamete to the female egg cell. A tightly controlled balance between cell wall deposition and internal pressure allows the pollen tube to rapidly reach the ovules for fertilization (Cameron and Geitmann, 2018).

In plants, the CWI signaling pathway serves to maintain mechanical homeostasis during cell expansion and in response to cell wall weakening (Gigli-Bisceglia *et al.*, 2020). Members of the *Catharanthus roseus* RLK1-like (CrRLK1L) protein family are proposed to sense wall conditions and transduce information to cytosolic signaling factors (Li *et al.*, 2016). The CWI signaling pathways in which CrRLK1Ls are involved are vital to maintaining cellular integrity in multiple processes, including pollen grain germination and pollen tube growth (Li *et al.*, 2016; Li and Yang, 2018; Ge *et al.*, 2019; Vogler *et al.*, 2019). In *Arabidopsis thaliana* pollen, ANXUR1 and ANXUR2 (ANX1/2) and Buddha's Paper Seal (BUPS)1/2 are membrane-localized CrRLK1L receptors. The ANX1/2–BUPS1/2 complex, as well as wall-anchored leucine-rich repeat extensins (LRX8/9/11), bind the autocrine small peptides known as rapid alkalinization factor (RALF) 4/19 to sense alterations in the cell wall. These signals are transduced to downstream signaling components, including the receptor-like cytoplasmic kinase MARIS (MRI), to regulate pollen tube growth rate and maintain cell integrity (Liao *et al.*, 2016; Li and Yang, 2018; Ge *et al.*, 2019). Mutants that disrupt the pathway, such as *anx1/2*, *mri*, *lrx8/9/11*, *bups1/2*, and *ralf4/19*, show increased grain bursting (Boisson-Dernier *et al.*, 2009, 2013, 2015; Miyazaki *et al.*, 2009; Liao *et al.*, 2016; Ge *et al.*, 2017; Fabrice *et al.*, 2018; Sede *et al.*, 2018) and some have elevated callose deposition (Fabrice *et al.*, 2018; Sede *et al.*, 2018). Overexpressing either *ANX1/2* or a dominant *MRI* allele (MRI^{R240C}) results in membrane invagination and hyperaccumulation of cell wall material (Boisson-Dernier *et al.*, 2013, 2015). MRI functions downstream of ANX1/2, as overexpression of MRI^{R240C} suppresses grain bursting in *anx1/2* mutants (Boisson-Dernier *et al.*, 2015).

It has been proposed that the CWI pathway could act in synergy with mechanosensitive channels, to integrate mechanical information from the cell wall and plasma membrane and maintain cellular mechanical homeostasis (Hamant and Haswell, 2017). The similar pollen bursting phenotypes of *msl8* mutants and CWI mutants support this idea. Here we further test this hypothesis with new mutant alleles of *MSL8* and two components of the pollen CWI pathway. Our data indicate a novel function for *MSL8* in cell wall organization during pollen germination and suggest a complex connection between *MSL8* and pollen CWI in maintaining cell integrity during germination.

Materials and methods

Plant growth

All the accessions used in this assay are Col-0 *A. thaliana* unless otherwise specified. Surface-sterilized seeds were plated on 0.5× Murashige and Skoog (MS) medium with appropriate antibiotics, incubated at 4 °C for 2

d, and then transferred to a long-day chamber (Percival) at 21 °C and 150 µmol at 53% relative humidity for 6–7 d before transplanting to soil (Pro-Mix PGX Biofungicide, Premier Tech Horticulture). Plants were grown in long days at 21 °C and 175 µmol at 45% relative humidity.

Generation and identification of CRISPR mutants

Plasmid pHEE401E with Cas9 (CRISPR-associated protein 9) driven by an egg cell-specific promoter (Wang *et al.*, 2015), and pCBC-DT1T2, which facilitates the cloning of two guide RNAs (gRNAs) (Xing *et al.*, 2014), were used for CRISPR/Cas9 gene editing as described (Xing *et al.*, 2014). Briefly, primers that harbored the two gRNA sequences targeting *MSL8* were used to amplify target fragments from pCBC-DT1T2, which was then introduced into pHEE401E yielding a destination construct for plant transformation. Two constructs, pHEE401E-MSL8_1e (LHP1198) and pHEE401E-MSL8_2e (LHP1199) (Supplementary Tables S1, S2), were made using this method, and were introduced into Col-0 and *msl7-1* mutant plants, respectively, by floral dip for *Agrobacterium*-mediated transformation (Clough and Bent, 1998). The transformants were screened on 0.5× MS plates supplemented with hygromycin (35 mg ml^{-1}, Gold Biotechnology, H-270-1). Candidates were screened for insertion/deletions (indels) by PCR amplification (Supplementary Table S1) and gel electrophoresis, then confirmed by sequencing. Cas9 in the selected lines was removed by backcrossing, and segregation in progeny was tested on antibiotic plates. Seedlings that showed hygromycin-sensitive growth were transferred to 0.5× MS plates without hygromycin for recovery, then transplanted to soil. The absence of Cas9 was further confirmed by genotyping. Alternatively, Cas9-free individuals in the segregating progeny were directly isolated by genotyping. Primers used to detect Cas9 and other genotyping information for the new *msl8* and *msl7 msl8* CRISPR alleles can be found in Supplementary Table S1.

Generation and identification of amiRNA mutants

A *MSL8* amiRNA cassette from pAmiR-MSL8 (CSHL_030627) was recombined into a pollen-specific expression construct (pB7WGLAT52, a gift from Gregory Copenhaver) using Gateway technology to make LAT52::amiRNA-MSL8. This construct was then introduced into the *msl7-1* mutant background by floral dip for *Agrobacterium*-mediated transformation (Clough and Bent, 1998). T1 lines were screened for Basta resistance. Candidates were further screened for silencing of *MSL8* gene expression by reverse transcription–PCR (RT–PCR) using RNA extracted from 15–30 newly open flowers. Duplicated below in semi-qTR-PCR section, which has more detailed information. The full sequence for amiR-MSL8 including attB sites is shown in Supplementary Table S2.

Generation and identification of LAT52::MRI^{R240C}–FP and LAT52::MSL8–YFP plants

LAT52::MRI^{R240C}–YFP (yellow fluorescent protein) and LAT52::MRI^{R240C}–CFP (cyan fluorescent protein) (Boisson-Dernier *et al.*, 2015) and LAT52::MSL8–YFP (Hamilton *et al.*, 2015) were introduced into *msl7-1 msl8-7* mutant plants or *anx1-2 anx2-1* homozygous plants (Boisson-Dernier *et al.*, 2009; Miyazaki *et al.*, 2009), separately, by floral dip for *Agrobacterium*-mediated transformation (Clough and Bent, 1998) and screened for Basta resistance. The primers for confirming the presence of either construct in plants are listed in Supplementary Table S1.

In vitro pollen germination and imaging

About 40 newly open flowers were collected into a 1.7 ml Eppendorf tube with 1 ml of pollen germination medium [PGM; 0.49 mM H_3BO_3, 2 mM $Ca(NO_3)_2$, 2 mM $CaCl_2$, 1 mM KCl, 1 mM $MgSO_4$, and 18% (w/v) sucrose with pH 7 adjusted with KOH (Bou Daher *et al.*, 2009)] and vortexed for 1 min before centrifugation at 10 000 *g* for 3 min at room temperature. Then the pollen pellet was rinsed with 20 µl of PGM, resuspended in 20 µl of fresh PGM, transferred to a polyethylenimine (PEI; Sigma-181978) pre-treated glass bottom microwell dish (MatTek, P35G-1.5-14-C), and dried until the grains were almost but not fully dry (1–5 min). Then 200 µl of PGM were gently added to the Petri dish, which was then placed in a humid box and incubated at 23 °C (incubator, VWR, 89511-416) for 4 h or 7 h. For PEI pre-treatment, the glass bottom of the dish was covered with 100 µl of diluted PEI (PEI:ddH_2O=1:30) for ~15 min before rinsing with 200 µl of ddH_2O twice. Then 200 µl of PGM was added for 15 min before rinsing again with ddH_2O and drying. Pollen germination images or movies were taken by Olympus IX73 microscope. For movies, 40× images were taken every 3 s for 5–45 min.

Pollen staining and imaging

Pollen viability staining was performed as described (Hamilton *et al.*, 2015) using pollen that was incubated in PGM for 2–3 h at 30 °C before staining. Aniline blue staining was performed according to Lu (2011) and Liu *et al.* (2016) using 0.01% decolorized aniline blue (DABS) (Sigma-Aldrich) solution with slight modifications. Pollen was germinated in a 1.7 ml Eppendorf tube with 200 µl of PGM for 4 h (Col samples) or 8 h (L*er* samples) at 23 °C before staining. Samples were stained in DABS for 4–6 h in the dark before imaging. Confocal images were collected on an Olympus FV3000 with the DAPI setting (excitation 405 nm and detection 430–470 nm).

Transmission electron microscopy

Pollen was collected and germinated in a 1.7 ml Eppendorf tube with 200 µl of PGM at 23 °C for 3.5 h (*msl7-1 msl8-7*) or 4.5 h [wild type (WT)]. Then pollen fixation and TEM were performed as described using a chemical fixation method for pollen grains (Jia *et al.*, 2017). After fixation, the following processes including infiltration, embedding, polymerization, ultrathin sectioning, staining, and TEM imaging were processed in the Center for Cellular Imaging (WUCCI) at Washington University in St. Louis. Grids with sections were examined using a JEOL JEM-1400 120 kV transmission electron microscope.

Immunoblot analysis

Freshly opened flowers of tested genotypes and the negative control were collected in a liquid nitrogen- (LN2) pre-treated Eppendorf tube and frozen immediately in liquid nitrogen. Ten-day-old seedlings of 35S::MSL10–green fluorescent protein (GFP) transformants (Veley *et al.*, 2014) were also collected as a positive control. Protein preparation, immunoblot with an anti-GFP antibody (1:5000 dilution, Takara Bio) followed by detection were performed as described (Basu *et al.*, 2020). Then the blot was stripped and re-probed with an anti-tubulin antibody (1:40 000 dilution, Sigma) for 0.5 h, followed by horseradish peroxidase (HRP)-conjugated goat anti-mouse secondary antibody (1:30 000 dilution; Millipore) with incubation for 0.5 h. Antibody incubations were all performed at room temperature. Detection was performed using the SuperSignal West Dura Detection Kit (Thermo Fisher) and Syngene PXi 4 imager with GeneSys software version 1.4.1.0 (Syngene).

Image analysis and processing

All image analysis and processing were performed in ImageJ (Fiji), PowerPoint, Adobe Photoshop CS6, or Adobe Illustrator 2019.

Statistical analysis

χ^2 test was carried out for all categorical datasets and ANOVA for the others using R (R Core Team 2020) (https://www.r-project.org/). Letters represent statistical differences adjusted for multiple comparisons using the false discovery rate (FDR) method for χ^2 test and Holm method for ANOVA test.

MSL7p::GUS reporter

For MSL7p::GFP–GUS, the promoter fragment was amplified from 3 kb upstream of *MSL7* using oligos LH722 and LH723 (Supplementary Table S1), cloned into pENTRY, sequenced, then recombined into pBGWFS7, trasnformed into plants, and selected with Basta. GUS staining was performed as described (Wang *et al.*, 2017). Images were taken on a stereoscope (Olympus SZX7) with a DP71 camera and/or a light microscope (Olympus, BX53) with DP80 camera.

Semi-quantitative RT–PCR

RNA was extracted by using either TRIzol Reagent (Invitrogen) or the RNeasy Mini RNA extraction kit (Qiagen) following the manufacturer's instructions. cDNAs were reverse transcribed from 1 µg of RNA using an oligo$(dT)_{20}$ primer and M-MLV Reverse Transcriptase (Promega). For RT–PCR, Taq polymerase and 1 µl of each cDNA were used in a 25 µl reaction. The corresponding primers for each target are listed in Supplementary Table S1. Thirty cycles of the following conditions were applied: 98 °C for 20 s, and 55 °C for 20 s, then 72 °C for 50 s. At1g13320, which is a housekeeping gene encoding the protein phosphatase 2A (PP2A) regulatory subunit, was used as an internal control (Czechowski *et al.*, 2005).

Results

Creation of new msl8 *and* msl7 msl8 *mutant lines*

We previously characterized pollen hydration and germination defects in two *MSL8* T-DNA insertion mutants (Hamilton *et al.*, 2015). However, the null *msl8-4* allele is in the Landsberg *erecta* (L*er*) background, while most mutants which can be sourced from publicly available stock centers are in the Columbia-0 (Col-0) background. Furthermore, *MSL8* (At2g17010) has a close homolog, *MSL7* (At2g17000), located in tandem on Chromosome 2 (Supplementary Fig. S1A). *MSL7* and *MSL8* have a partially overlapping expression pattern, as *MSL8* is expressed specifically in mature pollen gains and pollen tubes (Hamilton *et al.*, 2015) and an *MSL7p::GUS* reporter was expressed in pistil stigma cells and pollen tubes when grown through the stigma and style (Supplementary Fig. S1B, C), consistent with microarray data (Swanson *et al.*, 2005; Qin *et al.*, 2009). We thus identified *msl7-1* (SALK_133223) as a null T-DNA insertion allele in the Col-0 background (Supplementary Fig. S1A, G, H). We then used CRISPR/Cas9 gene editing of the *MSL8* gene to generate two null *msl8* alleles (*msl8-5* and *msl8-8*) and two double *msl7 msl8* mutants (*msl7-1 msl8-6* and *msl7-1 msl8-7*) in the Col-0 background (Supplementary Fig. S1D–F; Supplementary Table S1). We also used artificial miRNA (amiRNA)-based silencing to reduce *MSL8* transcripts in the *msl7-1* mutant background. Both *msl7-1 amiR-MSL8-1* and *msl7-1 amiR-MSL8-2* showed reduced *MSL8* transcript levels in flowers (Supplementary Fig. S1G, H; Supplementary Table S2).

We next germinated WT and mutant pollen grains *in vitro* and monitored their morphology after 4 h and 7 h. We observed increased pollen grain bursting (with the visible release of cytosol) at both time points, and increased germination rates at the earlier time point, in the single *msl8* and double *msl7 msl8* mutant lines when compared with pollen from WT or *msl7-1* single mutant plants (Fig. 1A). Similarly, pollen grains from *msl7-1 amiR-MSL8-1* and *msl7-1 amiR-MSL8-2* showed significantly more bursting and early germination compared with WT or *msl7-1* pollen grains (Supplementary Fig. S2A). There was no detectable difference between *msl8* single and *msl7 msl8* double mutant pollen in bursting or germination at either time point. The small but statistically significant difference in germination rates between *msl7-1* and WT pollen shown in Fig. 1A was not reproducible in other experiments (Supplementary Fig. S2).

Several novel pollen germination phenotypes are associated with msl7 msl8 *mutants*

A closer examination of germinated pollen grains from *msl8* and *msl7 msl8* CRISPR mutants revealed additional and unexpected phenotypes. Most WT germinated pollen grains were intact and produced a single pollen tube, while up to 50% of *msl8* and *msl7 msl8* mutant pollen grains either had burst but still had a growing tube or had germinated two tubes (Fig. 1A, B), which are collectively referred to here as 'abnormal germination'. The same abnormal germination phenotypes were observed in pollen from both amiR-*MSL8* lines (Supplementary Fig. S2B). These phenotypes could be ecotype dependent as they were not observed in the *msl8-4* mutant in the L*er* background.

To determine when bursting occurred in the *msl8* and *msl7 msl8* pollen, we performed time-lapse imaging of pollen grains in germination medium. In pollen from the mutants, but not from the WT, we observed several cases of burst pollen grains that later 'resurrected' an intact tube (Fig. 1C; Supplementary Videos S1–S3). We also observed examples of mutant grains with an intact tube producing a second growing tube (Supplementary Video S4). Thus, in some mutant grains, tubes could grow from grains that had burst before germination, and in some cases tubes could grow from grains that had already had a tube. To further explore this phenotype, we performed viability staining with fluorescein diacetate (FDA) for cell vitality and propidium iodide (PI) for membrane integrity (Boulos *et al.*, 1999; Muhlemann *et al.*, 2018). We found that 48% of burst *msl8* or *msl7 msl8* mutant pollen grains were still alive, compared with 23% of burst WT pollen (Fig. 1D). For all *msl8* mutant lines, the percentage of pollen that both burst and had a growing tube increased over time (Fig. 1A; Supplementary Fig. S2B). These observations suggest that grains lacking MSL8 have altered membrane and/or cell wall properties relating to turgor restoration and tube growth after grain bursting.

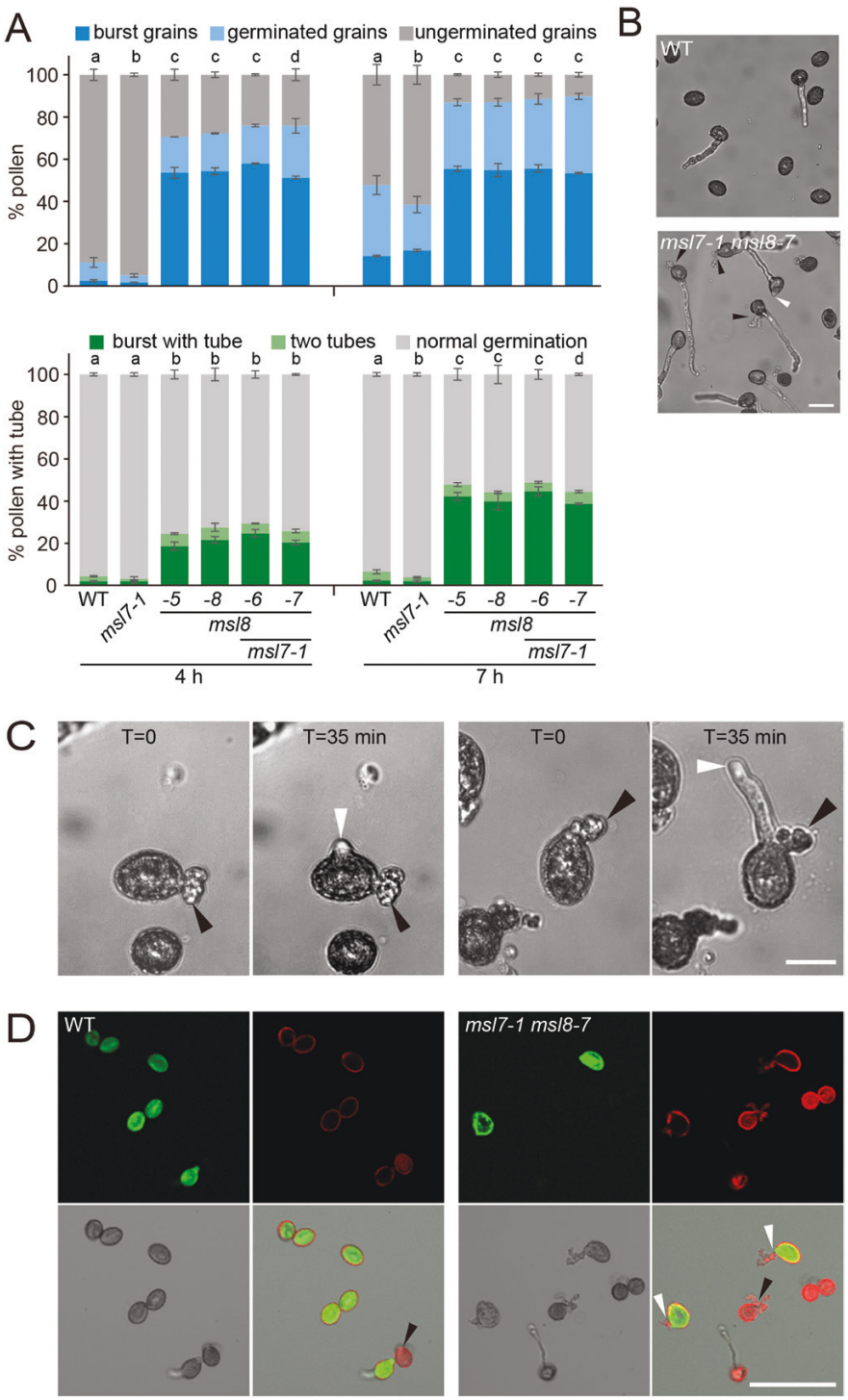

Fig. 1. Pollen from *msl8* mutants show multiple phenotypes during *in vitro* germination. (A) Top: bursting and germination rates at 4 h and 7 h after *in vitro* germination in the indicated genotypes. Averages from two experiments with n=1500–2000 grains per genotype per replicate are presented. Bottom: abnormal germination phenotypes at 4 h and 7 h. Averages from three experiments with n=100–300 grains per genotype per replicate at 4 h and ~500 grains at 7 h are presented. Error bars show the SEM. Statistical analysis, χ^2, P<0.001. (B) Brightfield images of pollen morphology after 4 h of *in vitro* germination. Black arrowheads indicate burst pollen grains with a tube; the white arrowhead shows two tubes from one pollen grain. Scale bar=50 µm. (C) Time-lapse images showing a burst pollen grain 'resurrecting' to germinate a tube from *msl7-1 msl8-6* (left two panels) and *msl7-1 msl8-7* (right two panels) pollen. Black arrowheads, sites of pollen grain bursting; white arrowheads, a pollen tube growing from a burst pollen grain. Scale bar=20 µm. (D) Confocal images of pollen after 2–3 h of *in vitro* germination in the indicated genotypes followed by viability staining. Green, fluorescein diacetate (FDA); red, propidium iodide (PI). White and black arrowheads indicate live and dead burst pollen grains, respectively. Scale bar=50 µm.

MSL8 is required for normal intine structure and callose deposition at the germination site

To investigate a possible novel role for MSL8 in controlling cell wall properties, we used TEM to examine the ultrastructure of germinating WT and *msl7-1 msl8-7* pollen grains (i.e. with visible protrusions ranging from a small bump to a fully extended tube). We did not see obvious differences between the two genotypes with respect to pollen coat or exine but did observe striking changes in the intine at the germination site (Fig. 2A). WT pollen had a relatively regular intine layer that thickened evenly at the germination site as reported previously (Hoedemaekers *et al.*, 2015). In *msl7-1 msl8-7* pollen, the intine was dramatically disrupted; in some cases, it was abnormally

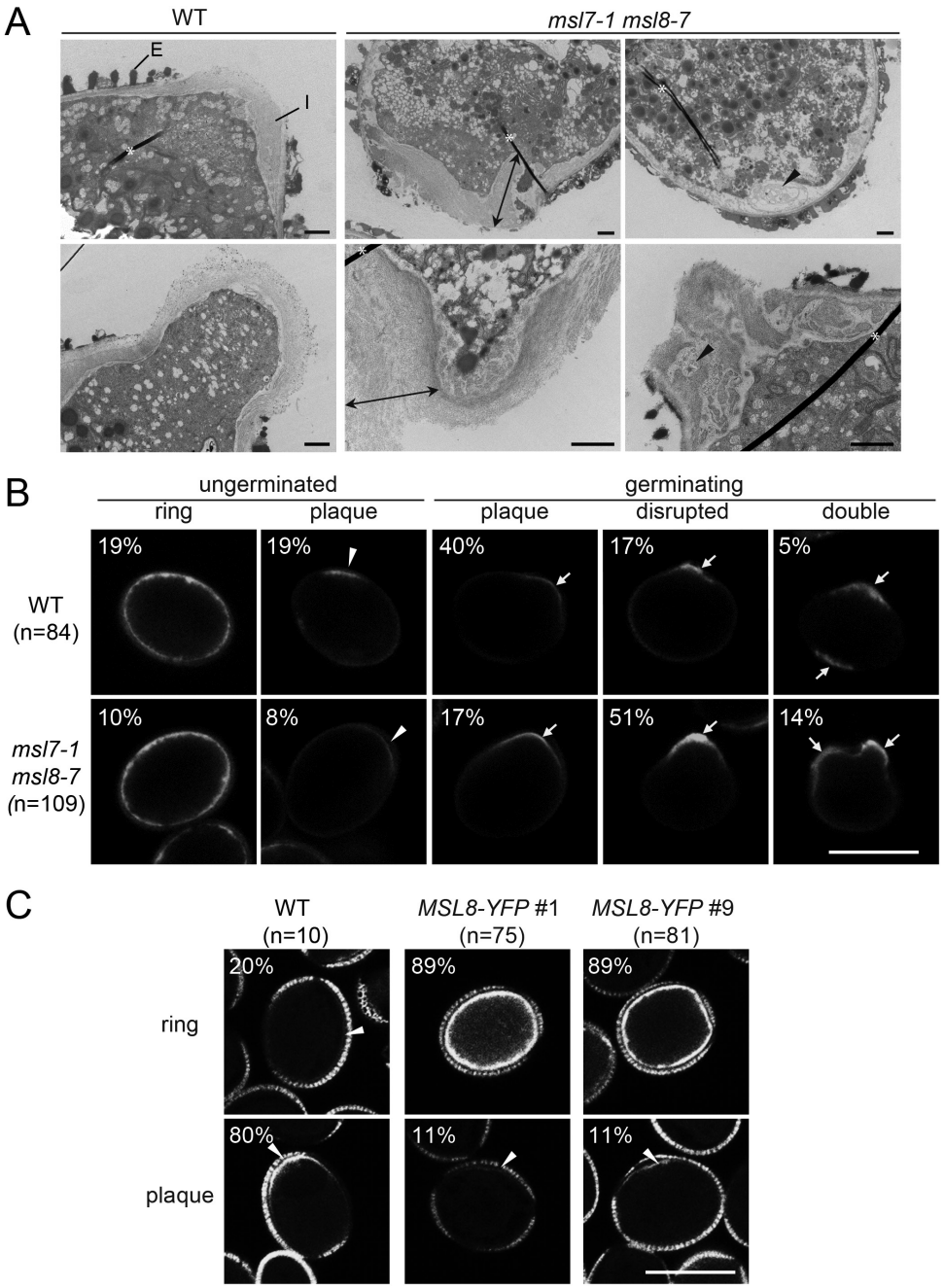

Fig. 2. MSL8 is required for normal formation of the germination plaque. (A) TEM images of germinating pollen grains from the indicated genotypes. In some cases, *msl7-1 msl8-7* grains exhibited extremely thick intine layers (double-headed arrows) and in others disrupted intine with occasional inclusions (black arrowheads). Asterisk, section artifact. E, exine; I, intine. Scale bar=1 μm. (B, C) Callose deposition in ungerminated or germinating pollen grains revealed by aniline blue staining. Due to very low germination rate in both MSL8–YFP lines, ungerminated and germinating pollen grains are combined (see text). Germination sites, white arrows; potential germination sites, white arrowheads. Scale bars=20 μm.

thick (two headed arrows), while in other cases it looked discontinuous or had inclusions (black arrowheads). The inclusion could be cytoplasm as previously reported (Hoedemaekers *et al.*, 2015). All these phenotypes indicate a role for MSL8 in establishing cell wall structure at the germination site.

We next used aniline blue staining to visualize callose deposition in germinating and ungerminated WT and *msl7 msl8* mutant pollen grains after 2–4 h incubation in germination medium (Fig. 2B). As mentioned above, callose deposition at the germination pore is important for hydration and germination (Johnson and McCormick, 2001; Hoedemaekers *et al.*, 2015). In both genotypes, many (mostly ungerminated) pollen grains remained unstained (81% in the WT and 67% in *msl7-1 msl8-7*, Supplementary Fig. S3A). A lack of signal in these experiments could reflect an inability to trigger callose deposition in preparation for germination (Johnson and McCormick, 2001) or differences in the ability to react with aniline blue. Among those grains that stained with aniline blue, 59% (19%+40%, ungerminated+germinating, Fig. 2B) of WT pollen grains showed a smooth callose plaque localized to the germination site or presumptive germination site, while only 25% (8%+17%, ungerminated+germinating, Fig. 2B) of stained pollen from *msl7 msl8* mutants did. Instead, the majority of these mutant pollen grains showed disrupted callose deposition, with an uneven, concentrated, or broadly distributed pattern at one (51%) or two sites (14%). A small portion of both genotypes (10–19%) showed a faint ring of callose around the grain (Fig. 2B).

We saw a different pattern in lines overexpressing *MSL8-YFP* from the strong, pollen-specific LAT52 promoter (*MSL8-YFP* hereafter) (Fig. 2C). Consistent with previous observations (Hamilton *et al.*, 2015), the majority of pollen grains from both *MSL8-YFP* overexpression lines were ungerminated even after 4 h incubation in PGM. However, 47–69% of these ungerminated grains had detectable callose, a much higher rate than in the WT (8%, Supplementary Fig. S3A). Furthermore, most MSL8–YFP pollen grains that did stain with aniline blue showed a strong ring of callose around the grain (89%, Fig. 2C). A small population of WT (20%) pollen grains showed a similar pattern (Fig. 2C). We saw similar callose patterns in the *msl8-4* mutant and *MSL8-YFP* lines in the L*er* background (Supplementary Fig. S4). These data show that MSL8 is involved in the formation of the germination plaque and suggest that defects in cell wall properties could contribute to the abnormal germination phenotypes shown in Fig. 1. While preliminary ruthenium red staining of pectin in pollen grains/tubes did not reveal reproducible differences between the genotypes, it remains possible that pectin modifications or other components of the pollen cell wall are affected by MSL8.

Overexpression of MRI^{R240C} *suppresses* msl8 *mutant phenotypes*

The discovery of defective pollen cell walls in the *msl7-1 msl8-7* mutant led us to hypothesize that the pollen CWI pathway might be disrupted in these lines. We predicted that increased grain bursting and other phenotypes of *msl8* and *msl7 msl8* mutant pollen might be suppressed if CWI signaling was enhanced. To test this, we overexpressed the gain-of-function *MRI* allele *MRI^{R240C}* in WT and *msl7-1 msl8-7* mutant plants. We identified three independent lines expressing YFP- or CFP-tagged *MRI^{R240C}* under the pollen-specific *LAT52* promoter (Twell *et al.*, 1990) in the *msl7-1 msl8-7* background (*msl7 msl8 MRI^{R240C}-FP)*. Both fluorescence imaging (Supplementary Fig. S5) and immunoblotting (Fig. 3A) indicated a range of expression levels; lowest in line 5, intermediate in line 4, and highest in line 14. All *msl7 msl8 MRI^{R240C}-FP* lines were backcrossed to WT plants, and siblings harboring homozygous *MRI^{R240C}-FP* in either the WT or the *msl7 msl8* background were isolated. As expected, in the WT background, intermediate and high expression of *MRI^{R240C}-FP* resulted in low bursting and low germination rates (Fig. 3B). Also as expected, *msl7 msl8* mutant pollen had high bursting and germination rates. Both phenotypes were significantly suppressed by intermediate and high *MRI^{R240C}-FP* overexpression at both 4 h and 7 h of incubation in germination medium. The low level of *MRI^{R240C}-FP* in line 5 also suppressed bursting and germination at the early time point, though not to WT levels. It is unclear why the low levels of *MRI^{R240C}-FP* in line 5 in the WT background had higher bursting rates than the WT. We further tested if the abnormal germination phenotypes observed in *msl7 msl8* were also suppressed by overexpression of *MRI^{R240C}-FP*. Indeed, expression of *MRI^{R240C}-FP* suppressed the abnormal germination observed in the *msl7 msl8* background in all three lines (Fig. 3C), primarily through reducing the rate of burst grains with a tube (Fig. 3C).

The effect of *MRI* on grain bursting and germination in *msl8* prompted us to characterize its effect on callose deposition. The proportion of pollen grains that did not stain with aniline blue was reduced in the *msl7 msl8* background (Supplementary Fig. S3B). As shown above, almost half of the *msl7 msl8* mutant pollen that stained with aniline blue had a disrupted plaque pattern of callose staining (Fig. 3D). About 30% of pollen grains overexpressing *MRI^{R240C}-FP* in the WT background exhibited a dramatic pattern of internalized callose staining (Fig. 3D). However, when *MRI^{R240C}-FP* was overexpressed in the *msl7 mls8* background, both the disrupted plaque phenotype of *msl7 msl8* and the internalized callose phenotype of *MRI^{R240C}-FP* were almost absent, and most pollen grains had either a localized callose plaque or a ring around the periphery similar to the pattern seen in the *MSL8–YFP* overexpression lines (Fig. 3D). Internalized callose was rarely observed in the WT or *msl7 msl8* mutant lines. Taken together, the data shown in Fig. 3 indicate that the genetic relationship between *MSL8* and *MARIS* is not linear and is likely to reflect complex biochemical or biophysical pathways.

Overexpression of MSL8-YFP *suppresses grain bursting in* anx1/2 *mutant pollen*

To further test for genetic interactions between *MSL8* and the CWI pathway, we overexpressed *MSL8-YFP* in the *anx1/2*

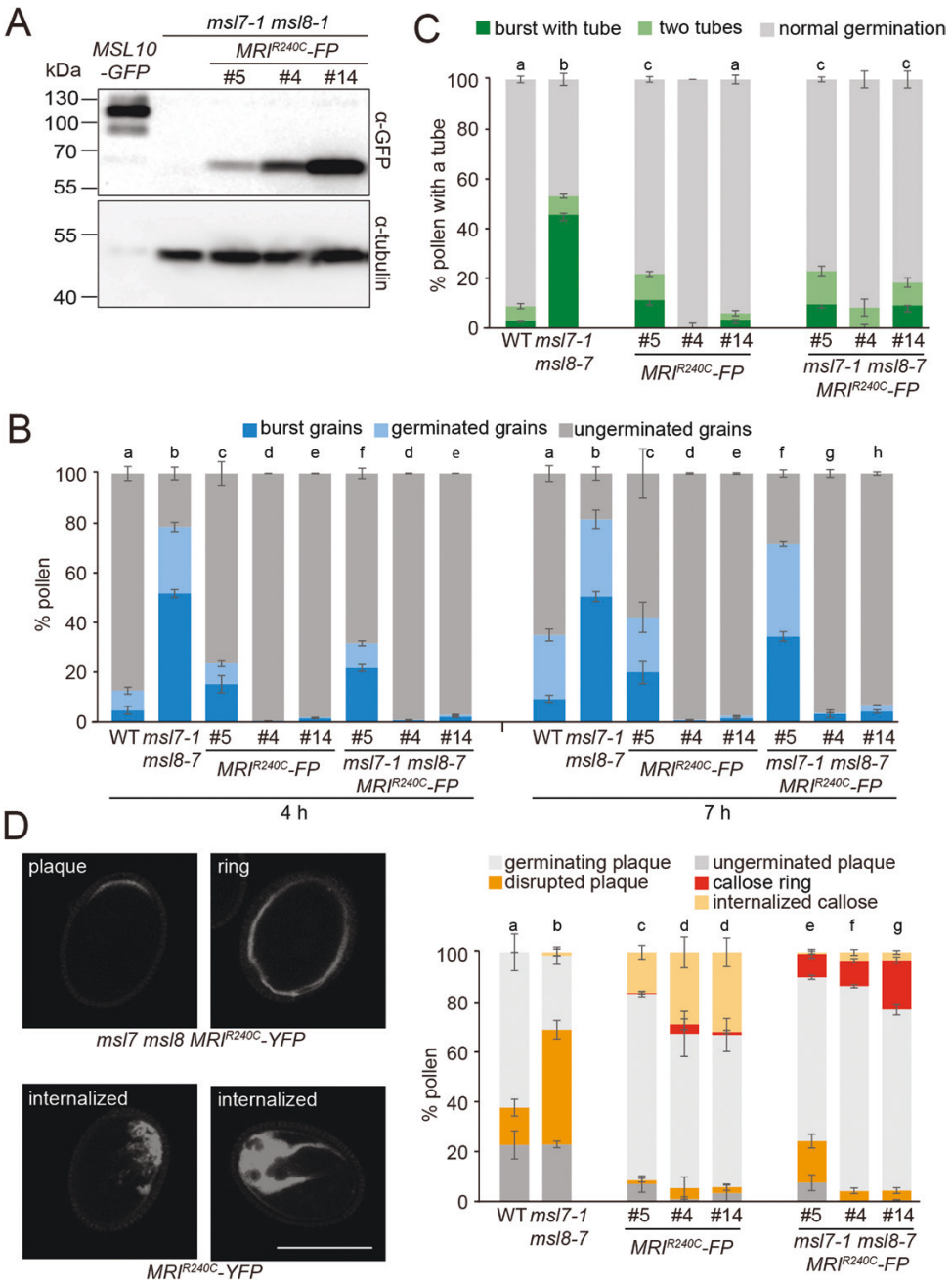

Fig. 3. *MARIS*^{R240C} suppresses grain bursting and germination rates and alters callose deposition in *msl7 msl8* mutant pollen. (A) Immunoblot of total protein from flowers of the indicated genotypes. 35S::MSL10–GFP (Veley *et al.*, 2014) was used as a positive control. The membrane was probed with anti-GFP antibody (upper panel) then stripped and re-probed with α-tubulin antibodies (bottom panel). (B) Pollen phenotypes during germination in the indicated genotypes. Averages from 3–6 experiments with *n*=1000–2000 grains per genotype per replicate are presented. Error bars show the SEM. (C) Abnormal pollen germination after 7 h in germination medium. Averages from 3–6 experiments are present. *n*=200–300 pollen tubes per replicate except for *MRI*^{R240C}-FP #4 (*n*=7), *MRI*^{R240C}-FP #14 (*n*=81), *msl7-1 msl8-7 MRI*^{R240C}-FP #4 (*n*=20), and *msl7-1 msl8-7 MRI*^{R240C}-FP #14 (*n*=175) due to low germination rates. Error bars show the SEM. (D) Left, representative aniline blue-stained pollen grains from the indicated genotypes. Scale bar=20 μm. Right, callose deposition pattern in the indicated genotypes. Only pollen grains with visible aniline blue stain are reported. Averages from 3–6 experiments with *n*=50–100 grains per genotype per replicate are presented. Error bars show the SEM. All *MRI*^{R240C} lines used in (A) were homozygous parental lines and in (B–D) were homozygous progenies isolated from the crosses between the WT and *msl7-1 msl8-7 MRI*^{R240C}. Statistical analysis in (B–D): χ^2 test, $P<0.05$. Because of low sample numbers, statistical analysis was not carried out for *MRI*^{R240C}-FP #4 or *msl7-1 msl8-7 MRI*^{R240C}-FP #4 in (C).

double mutant (*anx1/2 MSL8-YFP+/–*) and isolated two independent lines. The presence of YFP signal at the periphery and in internal puncta (as observed previously by Hamilton *et al.*, 2015) and immunoblotting indicated the presence of MSL8–YFP (Fig. 4A, B), but we were unable to isolate lines homozygous for the *MSL8-YFP* transgene, even after screening pollen from >50 T_2 individuals. Indeed, pollen from lines expressing *MSL8-YFP* in either the WT or the *anx1/2* background showed very low germination rates (Supplementary Fig. S6), as previously documented in the WT background (Hamilton *et al.*, 2015). We outcrossed both *anx1/2 MSL8-YFP+/–* lines to the WT and identified plants heterozygous for *MSL8-YFP* in the WT background.

We germinated parental and sibling pollen grains *in vitro* and examined their bursting rate (Fig. 4C). As expected, we observed a high degree of bursting in *anx1/2* double mutant pollen (~70%) (Boisson-Dernier *et al.*, 2009; Miyazaki *et al.*, 2009), while both *MSL8-YFP+/–* lines showed a very low burst rate (~8%) as previously described (Hamilton *et al.*, 2015). In both *anx1/2 MSL8-YFP+/–* lines, we observed an intermediate amount of bursting. We speculated that this might be due to the segregation of the *MSL8-YFP* transgene in the pollen grains. Therefore, we used fluorescence microscopy to identify pollen with or without YFP signal and compared the pollen bursting rate in each background at different time points from 8 h to 24 h. In pollen grains from *anx1/2 MSL8-YFP+/–* plants, the bursting rate in grains with YFP signal was always lower than in those without a clear YFP signal (Supplementary Fig. S7). It is worth noting that *anx1/2 MSL8-YFP* line #9 had much higher expression levels than line #1, but the two lines had similar effects on bursting and callose formation. One possible explanation is that the amount of *MSL8-YFP* overexpression that was obtained in line #1 is sufficient to fully produce these results;

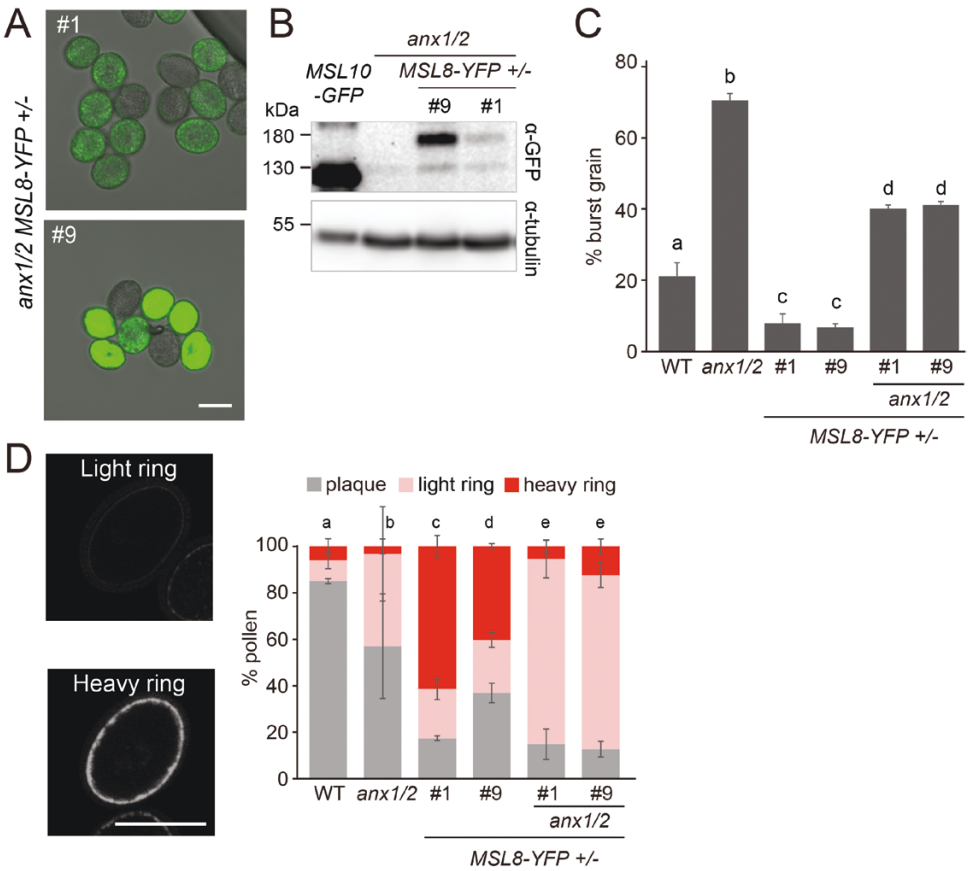

Fig. 4. Overexpression of *MSL8–YFP* suppresses grain bursting and alters callose deposition in *anx1/2* mutant pollen grains. (A) Merged fluorescent and brightfield images showing YFP signal in pollen from two independent *anx1/2 MSL8-YFP+/–* lines. Scale bar=20 μm. (B) Immunoblot of total protein from flowers of the indicated genotypes, performed as in Fig. 3A. (C) Pollen grain bursting rates at 24 h in the indicated genotypes. Averages from 3–7 experiments with *n* ~1000 pollen grains per genotype per replicate are presented. Error bars show the SEM. Statistical analysis: ANOVA test, $P<0.05$. (D) Left, representative images of callose deposition patterns in ungerminated pollen grains from *anx1/2 MSL8-YFP+/–* (top) or *MSL8-YFP+/–* (bottom) plants after aniline blue staining. Scale bar=20 μm. Right, callose deposition pattern in the indicated genotypes. Only pollen grains with visible aniline blue stain are reported. Averages from three experiments with *n* ~30–120 per genotype per replicate are presented, except for *anx1/2* (*n*=42 in total) due to high bursting rate. Error bars show the SEM. Statistical analysis: χ^2 test, $P<0.05$. *MSL8-YFP+/–* lines were derived from a cross between WT and *anx1/2 MSL8-YFP+/–* plants.

any additional expression obtained in line #9 does not have further effects.

To further characterize genetic interactions between *MSL8* and *ANX1/2*, we examined callose deposition in pollen grains from these lines by aniline blue staining. Since there were almost no intact germinating pollen grains in *anx1/2* mutant pollen, we focused on ungerminated pollen grains. As observed previously, not all pollen grains showed callose staining (Supplementary Fig. S3C). Additionally, the *anx1/2* alleles seemed to suppress staining even in the *MSL8-YFP* background (Supplementary Fig. S3C). Among the grains with callose signal, ~85% of WT and ~55% of *anx1/2* pollen grains showed a localized callose plaque (Fig. 4D). As above, overexpression of *MSL8-YFP* led to a heavy ring of callose around the pollen grain periphery. In *anx1/2 MSL8-YFP+/–* pollen grains, this ring was much fainter, suggesting that *ANX1/2* is partially required to produce the heavy callose ring in response to *MSL8-YFP* overexpression. Taken together, these findings further establish genetic interactions between *MSL8* and the pollen CWI pathway and suggest that they function in concert to maintain cell integrity during pollen germination.

Discussion

Plant cell expansion relies on a finely tuned balance between intracellular osmotic pressure and extracellular resistance from the cell wall, and dysregulation on either side of this equation can result in faulty growth behavior. In tip-growing cells, such as germinating and growing pollen tubes, the dynamic regulation of ion fluxes and of cell wall mechanical properties has been well studied, but mostly separately (Michard *et al.*, 2017; Cameron and Geitmann, 2018). The work reported here shows that these two key mechanical contributions are inter-related, providing a novel avenue of mechano-homeostatic feedback and growth regulation.

We have proposed that MSL8 functions as an osmotic valve (Basu and Haswell, 2017). According to this model, MSL8 is required to relieve internal pressure during pollen hydration and germination; in its absence, grains germinate more quickly and burst more readily. In overexpression lines, excess MSL8 releases pressure too efficiently, preventing the build-up of turgor that is required to drive germination. This 'osmotic safety valve' model for MSL8 function in pollen is complicated by the phenotypes and genetic interactions presented here. Consistent with previous work (Hamilton *et al.*, 2015), *msl8* or *msl7 msl8* mutants exhibited higher germination and bursting rates compared with the WT (Fig. 1A), while *MSL8-YFP* overexpression resulted in very low germination rates (Fig. 4C). However, we documented some new germination phenotypes, including double tubes and burst grains growing new tubes (Fig. 1A–C; Supplementary Fig. S2). It is worth noting that we cannot exclude the possibility that these phenotypes are general responses to germination stress, albeit more prevalent in *msl8* mutant pollen. A null *MSL7* allele did not affect any of these phenotypes.

Evidence for a new role for MS ion channels in cell wall organization

The fact that mutant pollen grains could burst and then recover and germinate a growing tube while WT grains that had burst rarely did so (Fig. 1D; Supplementary Videos S1-S3) suggested that there is more to MSL8 function than simply osmoregulation. Indeed, TEM and aniline blue staining showed that MSL8 is required for normal cell wall organization in ungerminated pollen grains and at the germination site (Fig. 2; Supplementary Fig. S4). Pollen from *msl8* mutants showed a disrupted and disorganized germination plaque and patchy callose deposition at the germination site (Fig. 2; Supplementary Fig. S4). Furthermore, the accumulation of callose in a ring at the periphery of ungerminated pollen was much more frequently observed and much more dramatic in pollen from *MSL8-YFP*-overexpressing plants than in pollen from the WT (Figs 2C, 4D; Supplementary Fig. S4). Thus, based on our TEM results and if the presence of callose can be used as a proxy for cell wall components, MSL8 unexpectedly modulates local cell wall organization in pollen grains before and during germination.

Genetic interactions between MSL8 and the CWI pathway are complex

MSL8's role in pollen integrity and cell wall deposition was at least superficially similar to that of the CWI pathway (Boisson-Dernier *et al.*, 2009, 2013, 2015; Miyazaki *et al.*, 2009), prompting us to test for genetic interactions between *MSL8* and two such components, *MRI* and *ANX1/2*. The results of these studies (summarized in Fig. 5A) do not easily conform to linear genetic pathways. The grain bursting and abnormal germination phenotype of *msl8* pollen was suppressed by overexpression of MRI^{R240C}*-FP* (Fig. 3A–C), while the grain bursting of *anx1/2* pollen was rescued by *MSL8-YFP* overexpression (Fig. 4A–C). In the *anx1/2* background, *MSL8-YFP* overexpression produced less intensely staining callose rings than they did in the *ANX1/2* background (Fig. 4D), suggesting that *ANX1/2* are required for the full effects of *MSL8-YFP* overexpression and that *MSL8* functions upstream of *ANX1/2*. However, other data suggest that *MSL8* acts downstream of or parallel to *ANX1/2*. For example, excess callose was deposited to the periphery whether or not *ANX1/2* were present in *MSL8-YFP*-overexpressing pollen (Fig. 4D).

Working model

Both MSL8 and the CWI pathway affect pollen germination, pollen bursting rate, and the pattern of callose deposition, and these phenotypes were affected in complex patterns that defy any linear relationship (Fig. 5A). As a result, we propose a simple model (Fig. 5B) wherein MSL8 and CWI signaling

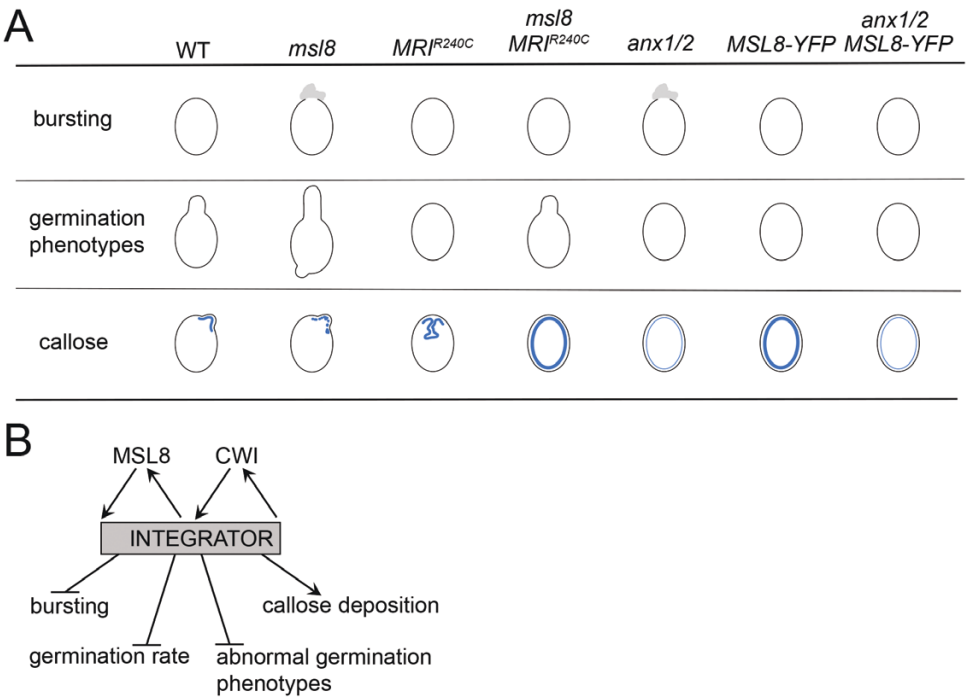

Fig. 5. Summary and model. (A) A chart summarizing typical phenotypes of the single and higher order mutants reported in this study, based on data shown in Figs 1A, 2B, C, 3B–D, 4C, D and Supplementary Fig. S6. (B) A simple model of the results presented here.

pathways are independent but impinge on a central common component, referred to here as an 'integrator', which can also feed back to either of them to ensure normal pollen germination and tube growth (Fig. 5B). This component could be a mechanical status, such as turgor, or a molecular signal, such as ions or reactive oxygen species, or a post-translational event, such as the formation of a complex. Future work is needed to determine the exact mechanism by which MSL8 and the CWI pathway interact and how their signals are translated into downstream effects.

Supplementary data

The following supplementary data are available at *JXB* online.

Fig. S1. *MSL7* expression pattern and *msl8* mutants generated by CRISPR/Cas9 and amiRNA.

Fig. S2. Abnormal germination in *msl7 amiR-MSL8* lines.

Fig. S3. Genotypic differences in pollen grain staining.

Fig. S4. Callose staining pattern due to *MSL8* loss of function or overexpression in the L*er* background.

Fig. S5. Fluorescence imaging in *MRI^{R240C}-FP* lines.

Fig. S6. Pollen germination rate in *anx1/2*, *MSL8-YFP*, and *anx1/2 MSL8-YFP* backgrounds.

Fig. S7. *MSL8–YFP* overexpression suppresses pollen grain bursting in *anx1/2*.

Table S1. Genotyping information.

Table S2. Sequence information for CRISPR and amiRNA constructs.

Supplementary References

Videos S1–S3. Burst pollen grains from the *msl7 msl8* mutant germinated a tube over time.

Video S4. A grain with a tiny tube produces a different tube that is growing.

Acknowledgements

We thank Dr Qi-jun Chen (China Agricultural University, China) for pHEE401E and pCBC-DT1T2; Dr Aurelien Boisson-Dernier (University of Cologne, Germany) for MRI^{R240C} constructs; Dr Hannes Vogler (University of Zurich, Switzerland) for *anx1-2 anx2-1* seeds; Dr Gregory Copenhaver (University of North Carolina at Chapel Hill, USA) for pB7WGLAT52; and the Center for Cellular Imaging at Washington University in St. Louis for TEM preparation, processing, and imaging.

Author contributions

YW and EH: designing the experiments; YW, JC, KM, and GJ: performing the experiments; YW, JC, and KM: data analysis; YW, EH, JC, and KM: writing.

Conflict of interest

The authors declare no competing interests.

Funding

This research was supported by National Science Foundation grants MCB-1253103 and MCB-1929355 (to ESH), National Science Foundation grant DGE-1745038 (to KM) and the National Science Foundation Center for Engineering Mechanobiology grant CMMI-1548571.

Data availability

The data that support the findings of this study are available from the corresponding author upon request.

References

Ackermann F, Stanislas T. 2020. The plasma membrane—an integrating compartment for mechano-signaling. Plants **9**, 505.

Adhikari PB, Liu X, Kasahara RD. 2020. Mechanics of pollen tube elongation: a perspective. Frontiers in Plant Science **11**, 1–13.

Basu D, Haswell ES. 2017. Plant mechanosensitive ion channels: an ocean of possibilities. Current Opinion in Plant Biology **40**, 43–48.

Basu D, Shoots JM, Haswell ES. 2020. Interactions between the N- and C-termini of the mechanosensitive ion channel AtMSL10 are consistent with a three-step mechanism for activation. Journal of Experimental Botany **71**, 4020–4032.

Bidhendi AJ, Geitmann A. 2019. Methods to quantify primary plant cell wall mechanics. Journal of Experimental Botany **70**, 3615–3648.

Boisson-Dernier A, Franck CM, Lituiev DS, Grossniklaus U. 2015. Receptor-like cytoplasmic kinase MARIS functions downstream of RLK1L-dependent signaling during tip growth. Proceedings of the National Academy of Sciences, USA **112**, 12211–12216.

Boisson-Dernier A, Lituiev DS, Nestorova A, Franck CM, Thirugnanarajah S, Grossniklaus U. 2013. ANXUR receptor-like kinases coordinate cell wall integrity with growth at the pollen tube tip via NADPH oxidases. PLoS Biology **11**, e1001719.

Boisson-Dernier A, Roy S, Kritsas K, Grobei MA, Jaciubek M, Schroeder JI, Grossniklaus U. 2009. Disruption of the pollen-expressed FERONIA homologs ANXUR1 and ANXUR2 triggers pollen tube discharge. Development **136**, 3279–3288.

Bou Daher F, Chebli Y, Geitmann A. 2009. Optimization of conditions for germination of cold-stored *Arabidopsis thaliana* pollen. Plant Cell Reports **28**, 347–357.

Boulos L, Prévost M, Barbeau B, Coallier J, Desjardins R. 1999. LIVE/DEAD BacLight: application of a new rapid staining method for direct enumeration of viable and total bacteria in drinking water. Journal of Microbiological Methods **37**, 77–86.

Cameron C, Geitmann A. 2018. Cell mechanics of pollen tube growth. Current Opinion in Genetics & Development **51**, 11–17.

Chen XY, Kim JY. 2009. Callose synthesis in higher plants. Plant Signaling & Behavior **4**, 489–492.

Clough SJ, Bent AF. 1998. Floral dip: a simplified method for *Agrobacterium*-mediated transformation of *Arabidopsis thaliana*. The Plant Journal **16**, 735–743.

Czechowski T, Stitt M, Altmann T, Udvardi MK, Scheible WR. 2005. Genome-wide identification and testing of superior reference genes for transcript normalization in Arabidopsis. Plant Physiology **139**, 5–17.

Fabrice TN, Vogler H, Draeger C, Munglani G, Gupta S, Herger AG, Knox P, Grossniklaus U, Ringli C. 2018. LRX proteins play a crucial role in pollen grain and pollen tube cell wall development. Plant Physiology **176**, 1981–1992.

Firon N, Nepi M, Pacini E. 2012. Water status and associated processes mark critical stages in pollen development and functioning. Annals of Botany **109**, 1201–1214.

Ge Z, Bergonci T, Zhao Y, *et al.* 2017. Arabidopsis pollen tube integrity and sperm release are regulated by RALF-mediated signaling. Science **358**, 1596–1600.

Ge Z, Cheung AY, Qu LJ. 2019. Pollen tube integrity regulation in flowering plants: insights from molecular assemblies on the pollen tube surface. New Phytologist **222**, 687–693.

Gigli-Bisceglia N, Engelsdorf T, Hamann T. 2020. Plant cell wall integrity maintenance in model plants and crop species-relevant cell wall components and underlying guiding principles. Cellular and Molecular Life Sciences **77**, 2049–2077.

Hamant O, Haswell ES. 2017. Life behind the wall: sensing mechanical cues in plants. BMC Biology **15**, 59.

Hamilton ES, Haswell ES. 2017. The tension-sensitive ion transport activity of msl8 is critical for its function in pollen hydration and germination. Plant & Cell Physiology **58**, 1222–1237.

Hamilton ES, Jensen GS, Maksaev G, Katims A, Sherp AM, Haswell ES. 2015. Mechanosensitive channel MSL8 regulates osmotic forces during pollen hydration and germination. Science **350**, 438–441.

Hoedemaekers K, Derksen J, Hoogstrate SW, Wolters-Arts M, Oh SA, Twell D, Mariani C, Rieu I. 2015. BURSTING POLLEN is required to organize the pollen germination plaque and pollen tube tip in *Arabidopsis thaliana*. New Phytologist **206**, 255–267.

Höfte H, Voxeur A. 2017. Plant cell walls. Current Biology **27**, R865–R870.

Jia PF, Li HJ, Yang WC. 2017. Transmission electron microscopy (TEM) to study histology of pollen and pollen tubes. Methods in Molecular Biology **1669**, 181–189.

Johnson MA, Harper JF, Palanivelu R. 2019. A fruitful journey: pollen tube navigation from germination to fertilization. Annual Review of Plant Biology **70**, 809–837.

Johnson SA, McCormick S. 2001. Pollen germinates precociously in the anthers of raring-to-go, an Arabidopsis gametophytic mutant. Plant Physiology **126**, 685–695.

Li C, Wu HM, Cheung AY. 2016. FERONIA and her pals: functions and mechanisms. Plant Physiology **171**, 2379–2392.

Li HJ, Yang WC. 2018. Ligands switch model for pollen-tube integrity and burst. Trends in Plant Science **23**, 369–372.

Liao HZ, Zhu MM, Cui HH, Du XY, Tang Y, Chen LQ, Ye D, Zhang XQ. 2016. MARIS plays important roles in Arabidopsis pollen tube and root hair growth. Journal of Integrative Plant Biology **58**, 927–940

Liu X, Castro C, Wang Y, Noble J, Ponvert N, Bundy M, Hoel C, Shpak E, Palanivelu R. 2016. The role of LORELEI in pollen tube reception at the interface of the synergid cell and pollen tube requires the modified eight-cysteine motif and the receptor-like kinase FERONIA. The Plant Cell **28**, 1035–1052.

Lu Y. 2011. Arabidopsis pollen tube aniline blue staining. Bio-Protocol **1**, 4–5.

Ma X, Wu Y, Zhang G. 2021. Formation pattern and regulatory mechanisms of pollen wall in Arabidopsis. Journal of Plant Physiology **260**, 153388.

Maksaev G, Shoots JM, Ohri S, Haswell ES. 2018. Nonpolar residues in the presumptive pore-lining helix of mechanosensitive channel MSL10 influence channel behavior and establish a nonconducting function. Plant Direct **2**, e00059.

Michard E, Simon AA, Tavares B, Wudick MM, Feijó JA. 2017. Signaling with ions: the keystone for apical cell growth and morphogenesis in pollen tubes. Plant Physiology **173**, 91–111.

Miyazaki S, Murata T, Sakurai-Ozato N, Kubo M, Demura T, Fukuda H, Hasebe M. 2009. ANXUR1 and 2, sister genes to FERONIA/SIRENE, are male factors for coordinated fertilization. Current Biology **19**, 1327–1331.

Monshausen GB, Haswell ES. 2013. A force of nature: molecular mechanisms of mechanoperception in plants. Journal of Experimental Botany **64**, 4663–4680.

Muhlemann JK, Younts TLB, Muday GK. 2018. Flavonols control pollen tube growth and integrity by regulating ROS homeostasis during high-temperature stress. Proceedings of the National Academy of Sciences, USA **115**, E11188–E11197.

Naismith JH, Booth IR. 2012. Bacterial mechanosensitive channels—MscS: evolution's solution to creating sensitivity in function. Annual Review of Biophysics **41**, 157–177.

Parre E, Geitmann A. 2005. More than a leak sealant. The mechanical properties of callose in pollen tubes. Plant Physiology **137**, 274–286.

Peyronnet R, Tran D, Girault T, Frachisse JM. 2014. Mechanosensitive channels: feeling tension in a world under pressure. Frontiers in Plant Science **5**, 558.

Qin Y, Leydon AR, Manziello A, Pandey R, Mount D, Denic S, Vasic B, Johnson MA, Palanivelu R. 2009. Penetration of the stigma and style elicits a novel transcriptome in pollen tubes, pointing to genes critical for growth in a pistil. PLoS Genetics **5**, e1000621.

Ranade SS, Syeda R, Patapoutian A. 2015. Mechanically activated ion channels. Neuron **87**, 1162–1179.

R Core Team 2020. R: A language and environment for statistical computing, Vienna, Austria: R Foundation for Statistical Computing.

Sede AR, Borassi C, Wengier DL, Mecchia MA, Estevez JM, Muschietti JP. 2018. Arabidopsis pollen extensins LRX are required for cell wall integrity during pollen tube growth. FEBS Letters **592**, 233–243.

Swanson R, Clark T, Preuss D. 2005. Expression profiling of Arabidopsis stigma tissue identifies stigma-specific genes. Sexual Plant Reproduction **18**, 163–171.

Trinh DC, Alonso-Serra J, Asaoka M, *et al.* 2021. How mechanical forces shape plant organs. Current Biology **31**, R143–R159.

Twell D, Yamaguchi J, McCormick S. 1990. Pollen-specific gene expression in transgenic plants: coordinate regulation of two different tomato gene promotors during microsporogenesis. Development **109**, 705–713.

Veley KM, Maksaev G, Frick EM, January E, Kloepper SC, Haswell ES. 2014. Arabidopsis MSL10 has a regulated cell death signaling activity that is separable from its mechanosensitive ion channel activity. The Plant Cell **26**, 3115–3131.

Vieira AM, Feijó JA. 2016. Hydrogel control of water uptake by pectins during in vitro pollen hydration of *Eucalyptus globulus*. American Journal of Botany **103**, 437–451.

Vogler H, Santos-Fernandez G, Mecchia MA, Grossniklaus U. 2019. To preserve or to destroy, that is the question: the role of the cell wall integrity pathway in pollen tube growth. Current Opinion in Plant Biology **52**, 131–139.

Wang Y, Tsukamoto T, Noble JA, Liu X, Mosher RA, Palanivelu R. 2017. Arabidopsis LORELEI, a maternally expressed imprinted gene, promotes early seed development. Plant Physiology **175**, 758–773.

Wang ZP, Xing HL, Dong L, Zhang HY, Han CY, Wang XC, Chen QJ. 2015. Egg cell-specific promoter-controlled CRISPR/Cas9 efficiently generates homozygous mutants for multiple target genes in Arabidopsis in a single generation. Genome Biology **16**, 144.

Wilson ME, Jensen GS, Haswell ES. 2011. Two mechanosensitive channel homologs influence division ring placement in Arabidopsis chloroplasts. The Plant Cell **23**, 2939–2949.

Xing HL, Dong L, Wang ZP, Zhang HY, Han CY, Liu B, Wang XC, Chen QJ. 2014. A CRISPR/Cas9 toolkit for multiplex genome editing in plants. BMC Plant Biology **14**, 327.

Xu T, Zhang C, Zhou Q, Yang ZN. 2016. Pollen wall pattern in Arabidopsis. Science Bulletin **61**, 832–837.